Integrative Multiomics and Drug Sensitivity Profiling Reveal Potential Biomarkers and Therapeutic Strategies in Pediatric Solid Tumors

Dina ElHarouni[1,2,3], Rosa Hernansaiz-Ballesteros[4], Heike Peterziel[1,5], Gnana Prakash Balasubramanian[1,2], Christopher Previti[1,2,6], Kathrin Schramm[1,7], Mirjam Blattner-Johnson[1,7], Rolf Kabbe[1,2], Barbara C. Jones[1,7,8], Sina Oppermann[1,5,9], David T.W. Jones[1,7,10], Stefan M. Pfister[1,2,8], Olaf Witt[1,5,8], Julio Saez-Rodriguez[4], Ina Oehme[1,5], Natalie Jäger[1,2], and Matthias Schlesner[11]

ABSTRACT

Cure rates for childhood malignancies using established therapy protocols have increased to an average of 80% but have reached a plateau. Moreover, survival rates are particularly low for some pediatric tumors—such as high-risk group 3 medulloblastomas, osteosarcomas, Ewing sarcomas, high-risk neuroblastomas, and high-grade gliomas—and dismal for patients with relapsed malignancies. A functional drug response profiling platform for pediatric solid and brain tumors has been established within the INFORM program to identify patient-specific vulnerabilities and biomarkers and to unravel molecular mechanisms associated with drug response profiles for clinical translation. In this study, we performed a multiomics analysis using drug sensitivity profiles, as well as genomic and transcriptomic data, of 81 pediatric solid tumor samples. The integrative analysis suggested two multiomics signatures associated with drug sensitivity. One signature distinguished neuroblastoma samples with sensitivity to navitoclax, a BCL2 family inhibitor. A second signature was specific to a subset of Wilms tumors harboring the *SIX1* (Q177R) hotspot mutation that displayed high expression of *MGAM*, *PTPN14*, *STAT4,* and *KDM2B* and high sensitivity to MEK inhibitors. A patient-specific causal interaction network analysis suggested possible molecular interactions between MEK inhibitors and the *SIX1* mutation in Wilms tumor samples. In conclusion, the integration of drug sensitivity profiling and multiomics data revealed potential biomarkers that may be associated with drug sensitivity in pediatric solid tumors. Patient-specific causal interaction network analysis further elucidated the interaction between inhibitors and signature biomarkers, providing insights that may inform clinical translation.

Significance: The combination of multiomics analysis and drug sensitivity profiling identified two signatures related to drug sensitivity in pediatric solid tumors, contributing to the advancement of functional precision medicine and personalized treatment strategies.

This article is part of a special series: Driving Cancer Discoveries with Computational Research, Data Science, and Machine Learning/AI.

Introduction

Childhood tumors, although constituting only about 1% of all tumor diagnoses, are the leading cause of disease-related death in children (1, 2). The genomic and transcriptomic landscape of pediatric cancers is significantly different from adult malignancies (3, 4). The clinical challenges of enormous inter-tumoral heterogeneity and occurrence of tumors that are (almost) never diagnosed in adults prompted the development of the first World Health Organization Classification of Pediatric Tumors (5). The classification is based on a multilayered strategy that considers the molecular profile, IHC, and the morphologic traits (5). Thus, molecular profiling enables a more fine-grained tumor classification (5) into molecularly defined subgroups with potential prognostic and sometimes predictive relevance (6).

[1]Hopp Children's Cancer Center Heidelberg (KiTZ), Heidelberg, Germany. [2]Division of Pediatric Neurooncology, German Cancer Research Center (DKFZ) and German Cancer Consortium (DKTK), Heidelberg, Germany. [3]Faculty of Biosciences, Heidelberg University, Heidelberg, Germany. [4]Faculty of Medicine and Heidelberg University Hospital, Institute of Computational Biomedicine, Heidelberg University, Heidelberg, Germany. [5]Clinical Cooperation Unit Pediatric Oncology, German Cancer Research Center (DKFZ), German Cancer Consortium (DKTK), and National Center for Tumor Diseases (NCT), Heidelberg, Germany. [6]Omics IT and Data Management Core Facility (ODCF), German Cancer Research Center (DKFZ), Heidelberg, Germany. [7]Division of pediatric Glioma Research Group, DKFZ, Heidelberg, Germany. [8]Department of Pediatric Oncology, Hematology and Immunology Heidelberg University Hospital and National Center for Tumor Diseases (NCT), Heidelberg, Germany. [9]Institute for Pharmacology and Clinical Pharmacy, Goethe University Frankfurt, Frankfurt, Germany. [10]National Center for Tumor Diseases (NCT), NCT Heidelberg, a partnership between DKFZ and Heidelberg University Hospital, Heidelberg, Germany. [11]Biomedical Informatics, Data Mining and Data Analytics, Faculty of Applied Computer Science and Medical Faculty, University of Augsburg, Augsburg, Germany.

N. Jäger and M. Schlesner contributed equally to this article.

Current address for D. ElHarouni: Dana Farber Cancer Institute, Boston, MA.

Corresponding Author: Dina ElHarouni, Dana Farber Cancer Institute, 450 Brookline Avenue, Boston, MA 02215. E-mail: dina_elharouni@dfci.harvard.edu

Cancer Res 2026;86:773–84

doi: 10.1158/0008-5472.CAN-24-1938

Historically, the advancement of treatments for pediatric cancers primarily concentrated on discovering and developing multimodal treatment regimens consisting of surgical resection, radiotherapy, and a combination of cytotoxic therapies alongside enhancing supportive care measures (7). Lately, the focus of innovation has shifted to mechanism-of-action–based drugs and immune-oncology approaches (8). In recent years, a significant advancement toward precision oncology in pediatric care has led to the initiation of numerous major national and international precision oncology programs. These initiatives have successfully enrolled thousands of participants, including children, adolescents, and young adults, marking a pivotal shift toward more mechanism-of-action–based therapeutic strategies (9). In these efforts, the potential of molecularly driven precision medicine was explored, and the clinical benefit of molecularly targeted therapies was evaluated (9).

Multiomics approaches have revolutionized precision oncology by leveraging genomic, transcriptomic, and proteomic data, enhancing tumor classification (10–12), and deepening our understanding of intra-tumor heterogeneity (13). Functional precision medicine has also proven feasible using organoids and patient-derived cells, which more accurately replicate patient-specific tumor environments and drug responses (14–16). Moreover, the integration of drug response profiling with multiomics data can improve the identification of potential therapeutic targets and specific vulnerabilities (17–19). Notably, although such integration has been explored in pediatric blood tumors (18), it remains less examined in pediatric solid tumors. Our study aims to fill this gap by applying these integrated approaches to pediatric solid tumors, potentially uncovering unique biomarkers.

The Individualized Therapy for Relapsed Malignancies in Childhood (INFORM) is an international precision oncology registry for children with high-risk relapsed/refractory malignancies (20, 21). The program aims to translate next-generation molecular diagnostics into biomarker-driven treatment strategies. By the data freeze of this study in January 2022, the INFORM registry included close to 2,000 patients, and more than 1,200 samples were molecularly profiled using next-generation sequencing [low-pass whole-genome sequencing, whole-exome sequencing (WES), and RNA sequencing (RNA-seq)] and microarray-based technologies (DNA methylation profiling). Within the INFORM program, an *ex vivo* functional drug sensitivity profiling (DSP) platform for pediatric solid and brain tumors has been established by the Hopp Children's Cancer Center Heidelberg Translational Drug Screening Unit, intending to complement the molecular profiles established in the context of the INFORM registry with functional drug sensitivity data for each patient. The DSP program aims to identify new biomarkers and molecular mechanisms associated with drug sensitivity profiles and foster direct clinical translation. By January 2022, the DSP program had screened tumors of 96 patients that were tested against a drug library of 79 clinically relevant drugs (Supplementary Table S1), using the laboratory protocol described recently by Peterziel and colleagues (22).

The pediatric INFORM registry was able to identify molecular drug targets in 50% of cases; however, only the 5% to 10% of cases with strong oncogenic drivers, including NTRK, BRAF, and ALK alterations, have so far been shown to benefit from molecularly matched targeted treatments (21). Of note, biomarkers for response prediction to frequently applied targeted drugs, including MEK, CDK, and mTOR inhibitors, are largely lacking (23). Hence, using the INFORM *ex vivo* drug sensitivity dataset, we aim to integrate the multiomics landscape of the tumors with their *ex vivo* drug sensitivity profiles to identify biomarkers and elucidate molecular mechanisms related to drug response. As an exploratory analysis, this study is intended to generate hypotheses and identify promising molecular and drug response signatures, laying the foundation for advances in pediatric precision oncology.

Materials and Methods

Ex vivo DSP

We screened 96 patient samples and 13 nonmalignant controls (astrocytes, fibroblasts, and peripheral blood smears) using an in-house protocol as described by Peterziel and colleagues (22). *Ex vivo* spheroids were cultured for 72 hours for all samples and seeded in round-bottom 384-well plates. All plates were screened for 79 clinically relevant drugs (Supplementary Table S1), each in five concentrations and in duplicates as previously described (24). ATP-based cell viability assay was performed using CellTiter-Glo 2.0 (G9243, Promega).

DSP analysis

iTReX (24) was used to analyze the raw viability drug screening data. iTReX analysis included the following steps: (i) normalization of raw viability measurements against positive and negative control wells of BztCl and DMSO, respectively, as described in (24). (ii) Quality control. As quality control parameters, the robust z prime, Pearson correlation between replicates, and the raw count values of the negative control wells were calculated and applied as described previously (22) to classify samples into "high-," "intermediate-," "borderline-," and "fail-" quality groups. Only intermediate- and high-quality screens were included into the downstream analysis of drug sensitivities.

(iii) Fitting of dose–response curves using a five-parameter logistic response model; and (iv) quantifying drug sensitivities using the asymmetric drug sensitivity score (DSS_{asym}) as described in (24). Selective drug sensitivity scores ($sDSS_{asym}$) were calculated by subtracting the mean of the nonmalignant controls from the DSS_{asym} of the tumor samples. A patient × drug $sDSS_{asym}$ matrix was prepared for further downstream analysis.

Variant calling

A DKFZ in-house workflow was used to process WES data of the INFORM registry study. Sequencing reads were aligned by the DKFZ One Touch Pipeline for both tumor and matching control samples against the human reference genome (build 37, version hs37d5; refs. 25, 26). Single-nucleotide variants (SNV) were identified using the SNVCalling workflow (version 1.2.166-3) based on samtools (27) and bcftools (28) with parameter adjustments and heuristic filtering as previously described by Jones and colleagues (29). Small insertion/deletions (InDels) were identified using the IndelCalling workflow (version 2.4.1) based on Platypus (30), in which the parameters applied were genIndels = 1, genSNPs = 0, ploidy = 2, and nIndividuals = 2. Variant call confidence was evaluated using Platypus, with only variants scoring a confidence between 8 and 10 considered. SNVs and InDels were functionally annotated using ANNOVAR (31). Variants reported in exac03 using ANNOVAR with a population frequency of 0.01 or higher, or annotated as "benign," "likely benign," or of "uncertain significance" in ClinVar, were excluded from our analysis.

Copy-number variation analysis

CNVkit (version 0.9.3; ref. 32) was used to call copy-number variations (CNV) from WES data using default parameters. Log_2 copy number ratio was used from the CNVkit cnr output files.

RNA-seq workflow

RNA-seq data were processed by the DKFZ One Touch Pipeline RNA-seq workflow (version 1.3.0; ref. 25). The RNA-seq read quality was evaluated using FastQC and the reads were mapped to the reference genome (hs37d5) using the STAR aligner (version 2.5.3a; ref. 33). Gene-level read quantification was performed using featureCounts (34), focusing on exon regions as defined in GENCODE v19 and considering both reads from each paired fragment with a stringent quality threshold of 255 to ensure unique alignments. Gene expression was computed as transcripts per million (TPM) values and z-transformed across the INFORM dataset.

Gene fusion calling

Gene fusions were identified in RNA-seq data using Arriba (version 1.0.1; ref. 35). Only gene fusions with high and medium confidence reported by Arriba were included for further analysis.

Multiomics factor analysis

The study employed a histology-agnostic analysis approach using multiomics factor analysis (MOFA+; ref. 36), which was applied across the full cohort of 76 samples with overlapping omics and drug sensitivity data. This strategy was designed to identify latent factors that could reveal both drug response patterns and tumor-specific signatures. The number of features in the molecular data views was reduced by retaining only events affecting oncogenic and/or druggable genes. We compiled a list of such genes as the union of genes that are (i) linked to cancer predisposition or progression (Catalogue of Somatic Mutations in Cancer v93; ref. 37), (ii) have actionable therapeutic implications (OncoKB v3.5; ref. 38), or (iii) have known drug–gene interactions (DGIdb 4.0; ref. 39). Each MOFA view was prepared as a matrix input with features as rows and sample IDs as columns as follows:

i. We prepared the gene expression matrix using the z-transformed TPM values from the RNA seq analysis, retaining only oncogenic and/or druggable genes. To further reduce the number of gene expression features, an elastic net regression model was trained between the gene expression features and the drug responses ($sDSS_{asym}$) to retain only gene features associated to drug responses. The positive weighted RNA features of the elastic net analysis were used for feature selection, only including features with a direct correlation with drug response data.
ii. Gene fusions were represented as binary matrix of individual genes. Medium- and high-quality gene fusions from the Arriba analysis were filtered to retain only oncogenic and/or druggable genes. As additional filtering step, genes that occurred as fusion partner in only a single sample were removed.
iii. Functional somatic variants (SNVs and InDels) were represented in a single binary matrix of genes. Genes in this matrix were filtered to retain only oncogenic and/or druggable genes and genes that were affected by functional somatic variants in at least two samples.
iv. CNVs were represented as binary matrix of individual genes. A matrix of CNVs was also prepared based on the preprocessed output of CNVkit. The matrix features were reduced to include oncogenic and druggable molecular events that are recurrent in at least two samples. The CNV matrix gene features were mapped to their corresponding cytogenetic bands using the Molecular Signatures Database (v7.0; refs. 40, 41) and the org.Hs.eg.db R package (42). Subsequently, we utilized the annotated genes for our analysis.
v. The drug response matrix was prepared using the selective drug sensitivity metrics ($sDSS_{asym}$). Drugs with zero variance across the dataset were excluded.

The multiomics model was computed using the R package MOFA+ (version 1.3.0; ref. 43) using a variance threshold of 2%, a convergence threshold of 0.01, and 20 random initializations. The model option likelihoods were set to "gaussian" for all data layer matrices and the parameters applied were spikeslab_factors = FALSE, spikeslab_weights = TRUE, ard_factors = FALSE, and ard_weights = TRUE. The model training arguments were set as follows: "1,000" maxiter iterations, "slow" convergence mode, startELBO = 1, freqELBO = 1, stochastic = FALSE, and verbose = FALSE. The highest evidence lower bound value was selected for downstream analysis.

MOFA+ factors selection and downstream analysis criteria

Factors were filtered based on their contribution to the variance in drug sensitivity data (sDSS_asym). A cutoff of ≥5% variance explained was applied to identify factors of biological significance. Only factors exceeding a 10% variance drug response threshold were prioritized, ensuring the identification of meaningful sensitivity patterns.

To validate the identified factors, we analyzed the weights of drug response features contributing to each factor. Factors 1 and 3 were prioritized based on the presence of high-weight drugs (weights >0.7), indicating stronger contributions to variance explained. Supplementary Fig. S1A illustrates the association of factor 1 with MEK inhibitors (MEKi) and chemotherapeutics and factor 3 with BCL2 inhibitors, highlighting their roles in oncogenic signaling and apoptosis regulation, respectively. Lower-weight factors (e.g., factors 2, 5, and 9) were deprioritized for downstream interpretation because of reduced influence on drug response variance.

Pathway activity analysis

Pathway footprints were identified from gene expression (RNA-seq) data using PROGENy (Pathway RespOnsive GENes; version 1.10.0; ref. 44). PROGENy is specifically designed to estimate pathway activity from gene expression data and includes a predefined set of 14 signaling pathways. Pathway activity scores were computed using the normalized TPM expression values of the 100 most significant genes per pathway while setting the model organism to "Human" (44).

Transcription factor activity

We computed transcription factor (TF) activity scores from gene expression TPM values using the DoRothEA R package (version 1.0.1; ref. 45). TF target interactions with confidence levels A, B, and C were selected, resulting in 289 TF regulons. VIPER (version 1.22.0) was used to run DoRothEA, in which the scaled method was used for computing the single-sample signatures and a minimum of four targets were allowed per regulon.

CARNIVAL analysis

CARNIVAL (version 1.0.0; ref. 46) was used to contextualize our functional drug response profiles and omics data into a causal network. A sample-specific prior knowledge network was constructed using a constraint setting based on the patient's genomic profile (functional SNV, InDel mutations, and fusions). The prior knowledge was curated using the OmniPath (47) R package

"import_all_interactions" function. CPLEX solver was used to solve the optimization problem.

Results

Integrated analysis of drug screening and omics data reveals subsets of tumors with specific therapy sensitivities

High-throughput testing of a library of 79 compounds (Supplementary Table S1) was used to establish the *ex vivo* drug sensitivity profiles for 96 INFORM pediatric solid and brain tumors (**Fig. 1A**). Following the drug screening quality control criteria (22), we classified 47 drug screens as high quality and 34 as intermediate quality (**Fig. 1A**), whereas 15 samples exhibited borderline or low quality and were excluded from further analyses. The 81 samples included for further analysis belong to 24 molecular subgroups of various cancer entities (**Fig. 1A**; Supplementary Table S2). Sensitivity was assessed based on the selective drug sensitivity score ($sDSS_{asym}$) metric (24), which takes into consideration the efficacy of the drug on the specific tumor tissue and the toxicity of the drug in a non-malignant tissue of a reference control (**Fig. 1B**). Drug sensitivity patterns were clustered column-wise based on the similarity of response across samples and clustered row-wise based on the sensitivity profile of the drug across the cohort (**Fig. 1B**). Clustering of tumors by drug sensitivity profiles revealed similar drug sensitivity patterns for Ewing sarcomas and for ependymomas, a rare brain tumor type. Other entities, such as Wilms tumor, showed more than one cluster of drug sensitivity patterns, which indicates molecular diversity within the tumor type, thus increasing the potential to identify druggable targets for such clusters.

To explore the combined variability of phenotypic drug screens and omics data, we gathered omics data comprising five different data layers (also termed "data views"; **Fig. 2A**) for the investigated INFORM samples, resulting in 76 samples with data intersections between drug screens and omics data. The data views included functional small somatic mutations (SNVs/InDels), genomic CNVs, gene expression values (RNA), gene fusions, and drug response profiles ($sDSS_{asym}$ metrics; **Fig. 2B**). We used MOFA+ (36), a multiomics factor analysis tool, to decompose the different data layers using matrix factorization. The trained model captured nine MOFA latent factors, in which each factor represents a minimum of 5% variance in at least one data layer (**Fig. 2B**). The cumulative variance explained for each of the nine factors was distributed in the data views as follows: 39% of variance in the RNA expression data, 29% in the drug response layer, 15% in gene fusions, 9% in CNVs, and 5% in the mutations layer (**Fig. 2C**).

In the MOFA+ analysis, each "factor value" represents the activity level of a given latent factor for a particular sample. Higher factor values signify increased activity or influence of that factor on the sample and *vice versa*. By examining the distribution of samples for each factor (**Fig. 2D**), we discerned four entity-specific factors (1, 2, 3, and 5). Notably, two of these factors (1 and 3) accounted for a considerable portion of the variance within the drug response data layer. Factor 1 was mainly driven by Wilms tumor samples, whereas factor 3 had the top weight inferred by neuroblastoma samples.

Factors 2 and 5 showed entity-specific sample contribution toward Ewing sarcoma and BCOR sarcoma, respectively (**Fig. 2D**). Both factors had a strong contribution of gene fusions to their variance (**Fig. 2B**). Based on the top weights in the fusion data layer, factor 2 was driven by the occurrence of the pathognomonic *EWSR1* fusion of Ewing sarcoma (Supplementary Fig. S1B), whereas factor 5 was driven by the *BCOR* fusion, which is defining BCOR sarcomas (Supplementary Fig. S1C). Within our MOFA+ analysis, gene fusions were treated as individual genes. For each factor, the gene with the second-highest weight reported was the most frequent fusion partner gene in the well-known pathognomonic fusion, such as *EWSR1-FLI1* and *BCOR-CCNB3*.

We explored features with the highest weights in the data layers that showed significant variability, specifically focusing on factors that were closely associated with high variance in drug response profiles. Factors 1 and 3 were the only two factors with a contribution from the drug sensitivity layer explaining more than 10% of the total variance (**Fig. 2B**). Factor 3 was dominated by four neuroblastoma samples, whereas factor 1 was dominated by three Wilms tumor samples (**Fig. 2D**). Factor 3 explained almost exclusively variance in the drug sensitivity and the gene expression layers. Top-weighted features within this factor were the sensitivity to navitoclax (a BCL2 family inhibitor) and the high expression of a set of three genes (*DUSP8*, *GATA3*, and *PHOX2B*; **Fig. 2E**). Factor 1 explained high variance across three data layers: drug sensitivity ($sDSS_{asym}$), mutations, and RNA expression. The top-weighted drug feature in factor 1 was sensitivity to trametinib (a MEKi; **Fig. 2F**). Moreover, the factor had *SIX1* mutations as the top-weighted feature within the mutation data layer, and a gene expression signature in the RNA expression value layer comprised by high expression of *MGAM*, *PTPN14*, *STAT4*, and *KDM2B* (**Fig. 2F**). In summary, our integrated analysis of drug sensitivity and omics data identified a subset of neuroblastoma, characterized by high expression of *DUSP8*, *GATA3*, and *PHOX2B*, and sensitivity to the BCL2 family inhibitor navitoclax. In addition, we identified a subset of Wilms tumors harboring the *SIX1* (Q177R) hotspot mutation, which showed high expression of *MGAM*, *PTPN14*, *STAT4*, and *KDM2B* and high sensitivity to all three MEKi represented in the drug library (trametinib, cobimetinib, and selumetinib). These results indicate a possible association between specific omics-based features and sensitivity to navitoclax in neuroblastoma and MEKi in Wilms tumors.

The selective sensitivity of a Wilms tumor subset correlates with distinct omics features

To elucidate whether the distinct omics features identified confer selective sensitivity to BCL2 and MEKi in neuroblastoma and Wilms tumors, respectively, we visualized the correlation of the top gene expression features present with the drug response–related latent factors (factor 1 and 3; **Fig. 3A** and **B**). We investigated the association between SIX1 (Q177R) mutation status and sensitivity to MEKi (trametinib, cobimetinib, and selumetinib) in Wilms tumors. The analysis revealed significant differences in drug sensitivity, with P values of <0.0001 for trametinib, 0.003 for cobimetinib, and 0.006 for selumetinib (Supplementary Fig. S2A). We also analyzed the association between the selective sensitivity to MEKi and the expression levels of the four identified genes (*MGAM*, *PTPN14*, *STAT4*, and *KDM2B*) in our cohort (**Fig. 3A**), together with the SIX1 mutation status. This analysis demonstrated a specific association between the SIX1 mutation (present in a subset of Wilms tumors), gene expression, and MEKi sensitivity in our cohort (**Fig. 3A**).

To validate these findings, we analyzed an independent pediatric Wilms tumor dataset from the TARGET cohort (3). The cohort included $n = 101$ Wilms tumor samples, of which, four harbored the SIX1 (Q177R) mutation. A significant increase in the expression of three genes (*MGAM*, *KDM2B*, and *STAT4*) was observed in the SIX1-mutated samples compared with SIX1 wild-type cases (P values: 0.003, 0.0045, and 0.0037, respectively; Supplementary Fig. S2B). Although

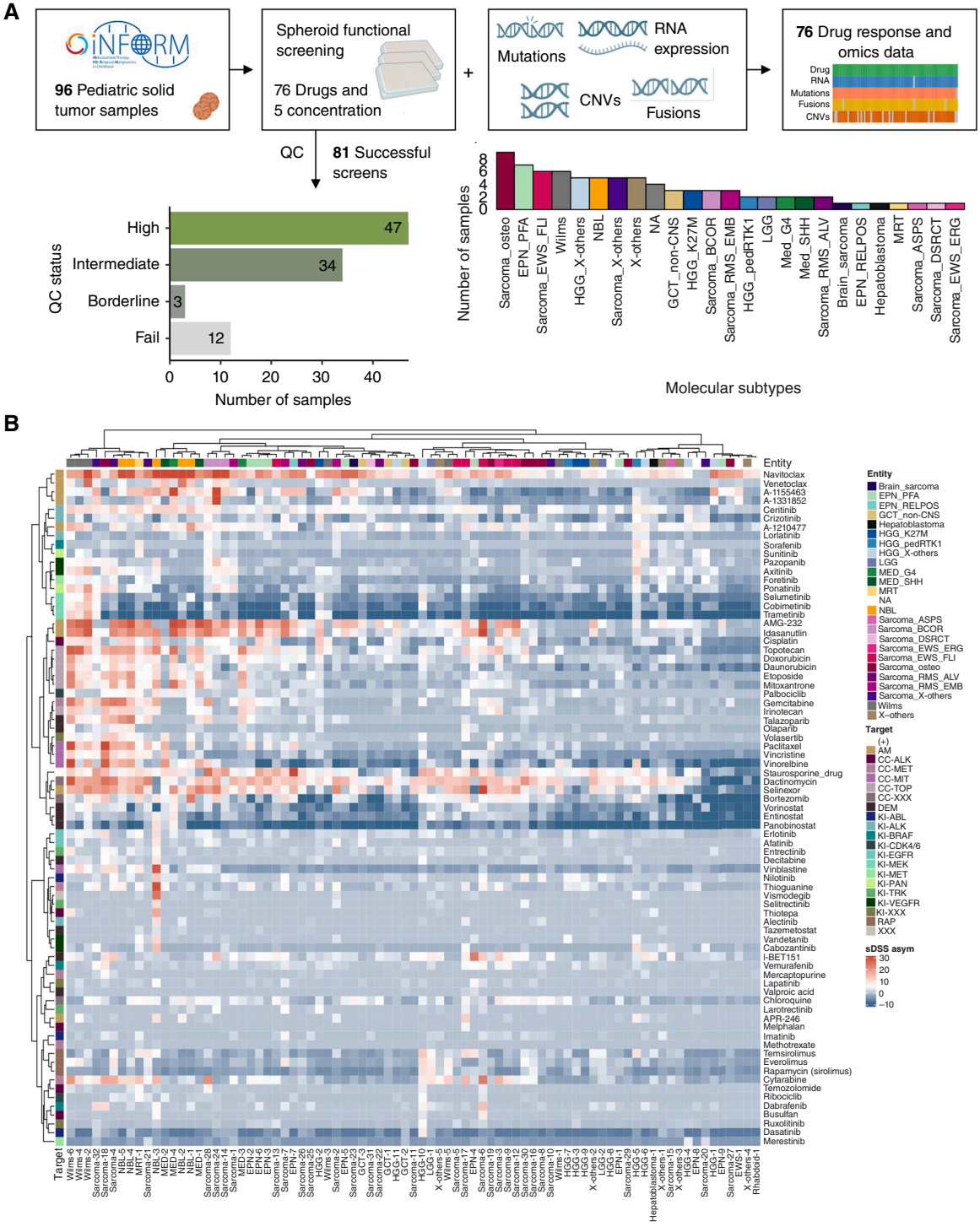

Figure 1.

Functional drug screening and multiomics in pediatric solid tumors from the INFORM registry. **A,** Schematic diagram of the INFORM multiomics and functional drug screening workflow. The diagram includes the number of samples per quality control (QC) classification class (high, intermediate, borderline, and fail) of *ex vivo* drug screens. Only high- and intermediate-quality samples were included in further analyses. The diagram further includes the number of samples per cancer molecular subgroup in the INFORM drug screening dataset passing quality control (high and intermediate quality; $n = 81$). Abbreviations of the molecular subgroups are described in Supplementary Table S2. **B,** Heatmap showing the *ex vivo* drug sensitivity (red) or resistance (blue) based on the $sDSS_{asym}$ metric across the INFORM drug screening dataset ($n = 81$). Gray cells correspond to missing values. Clustering is based on Euclidean distance (rows) and Kendall distance (columns). Rows are annotated with the drug target class (left) and columns are annotated with the cancer molecular subgroup (top). Mapping of INFORM IDs to sample identifiers (*x*-axis) is described in Supplementary Table S3.

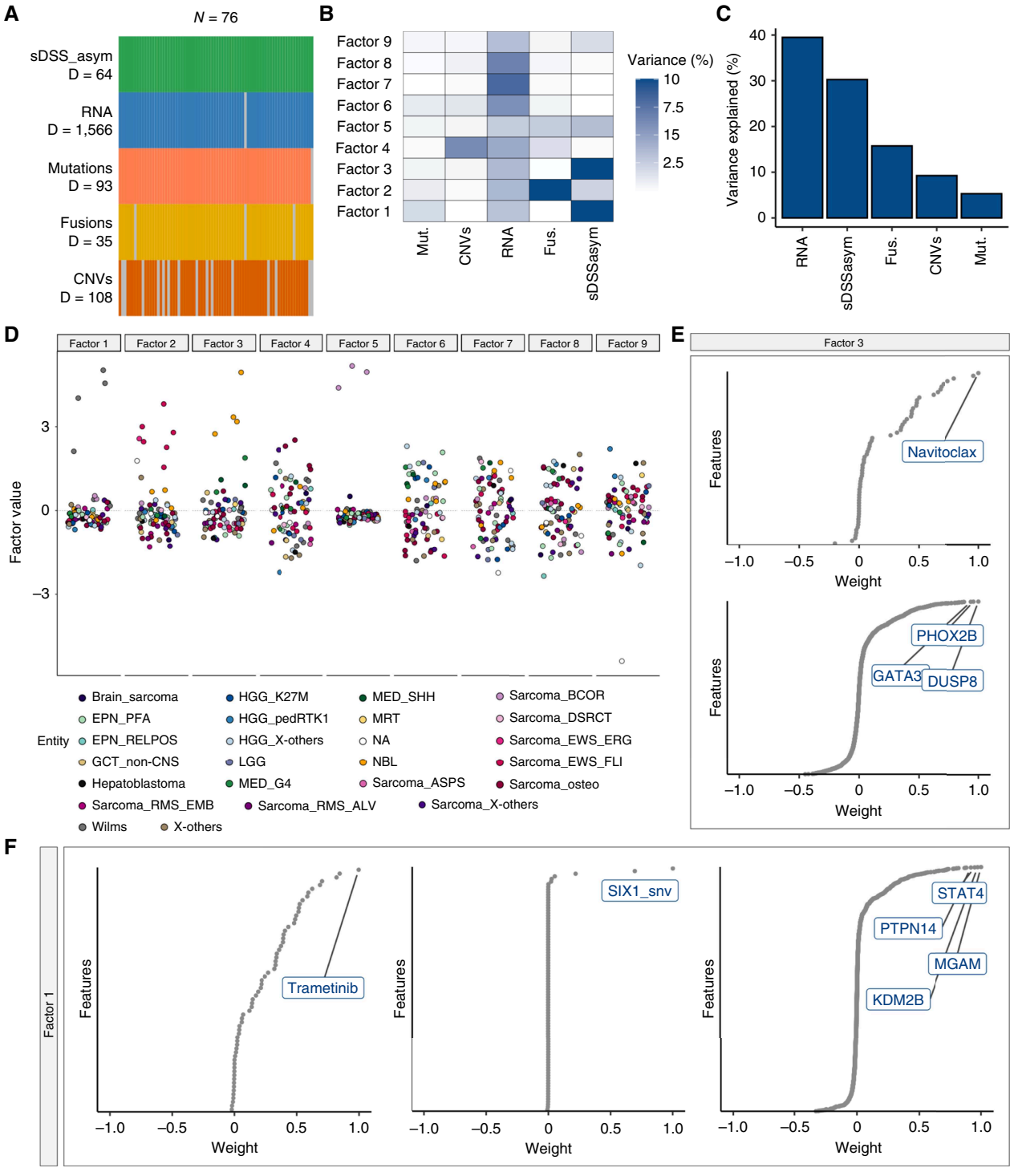

Figure 2.

The INFORM MOFA+ model. **A,** Dataset for the MOFA+ analysis. Data modalities are shown in different rows (D = number of features) and samples (*N*) in column, in which gray bars indicate missing data for the respective sample. **B,** Variance explained by the nine factors of the MOFA model for each data layer. **C,** Percentage of total variance explained by individual factors for each data layer. **D,** Sample factor values per factor. Each dot represents an INFORM sample, with the color indicating the tumor entity. **E,** Top weighted features from high variability data views (drug response and RNA expression) of factor 3. **F,** Top weighted features from high variability data views (drug response, genomic mutation, and RNA expression) of factor 1. A positive factor value signifies an elevated expression or activity of a particular feature in samples. Conversely, a negative factor value indicates reduced expression or activity of that feature.

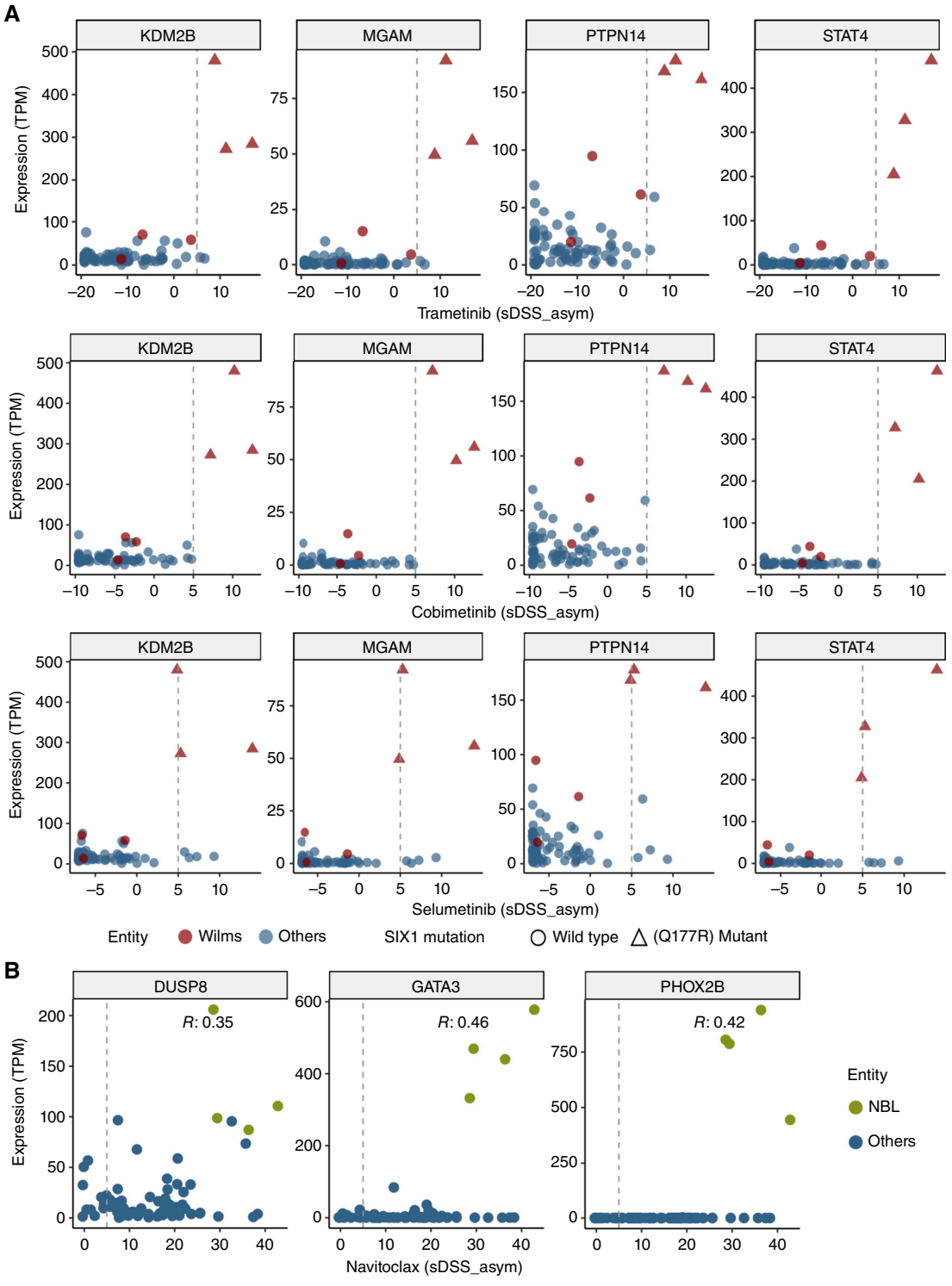

Figure 3.

Correlations of drug response signature biomarkers. Scatterplots illustrating the correlation between gene expression levels (TPM) and selective drug sensitivity scores (sDSS_asym) across Wilms tumor and neuroblastoma samples. **A,** Expression of *KDM2B*, *MGAM*, *PTPN14*, and *STAT4* genes in Wilms tumor samples correlates with sensitivity to MEKi (selumetinib, cobimetinib, and trametinib). Distinct sensitivity patterns for SIX1 wild-type (circle) and SIX1 (Q177R)-mutant (triangle) Wilms tumors are visualized. Wilms tumor samples are annotated in red and categorized by SIX1 mutation status, whereas other entities in the cohort are displayed in blue for comparison. An sDSS_asym of 5 is visualized as the threshold used to define drug sensitivity. **B,** Expression of *DUSP8*, *GATA3*, and *PHOX2B* genes in neuroblastoma samples shows no significant correlation with sensitivity to the BCL2 inhibitor navitoclax.

PTPN14 exhibited higher expression in SIX1-mutated samples, the difference was not statistically significant, potentially reflecting heterogeneity in its expression or a less robust association. This independent validation reinforces the association between SIX1 mutation status and the expression of these genes, although additional studies are needed to establish their predictive value in Wilms tumors.

Similarly, we explored the correlation between navitoclax sensitivity and the expression levels of a set of genes in neuroblastoma samples. Although navitoclax sensitivity and expression of the three genes was high in the neuroblastoma samples, none of the genes demonstrated a significant correlation with navitoclax sensitivity, suggesting that the sensitivity captured in our dataset is not directly linked to specific gene expression features (**Fig. 3B**).

To validate the observed drug sensitivity features in neuroblastoma, we extended our analysis to the neuroblastoma cell line data within the GDSC2 dataset. To assess the similarity between neuroblastoma cell lines and primary tumor tissues, we used the Cancer Dependency Map (Celligner) algorithm to identify neuroblastoma samples with the nearest transcriptional distance to tumor tissue (Supplementary Fig. S3A). This analysis identified 19 neuroblastoma cell lines with transcriptional profiles concordant with tumor tissues from The Cancer Genome Atlas cohort. These neuroblastoma cell lines exhibited a significantly higher mean expression of *GATA3* and *PHOX2B* compared with all other entities within the Cancer Dependency Map portal (Supplementary Fig. S3B). A two-way comparative analysis of drug responses using GDSC2 AUC values revealed that BCL2 family inhibitors (navitoclax and ABT737) were among the top selective drug sensitivities in neuroblastoma cell lines (Supplementary Fig. S3C). Navitoclax responses in neuroblastoma models displayed a distinct AUC distribution compared with other cancer types, suggesting a lineage-associated drug sensitivity pattern (Supplementary Fig. S3D). Additionally, neuroblastoma cell lines were selectively sensitive toward alisertib (AURKA inhibitor), MST 312 (telomerase inhibitor), and APO 866 (NAMPT inhibitor) in the GDSC2 dataset; however, these compounds were not included in the INFORM drug library (Supplementary Table S1). While comparing drug sensitivity with the gene expression signature in neuroblastoma using the GDSC2 dataset, no correlation was observed between the two events (Supplementary Fig. S3E). This finding reveals that although BCL2 family inhibitor sensitivity and high gene expression are both relevant in neuroblastoma, they are independent phenomena. These results highlight that the gene expression features identified are not predictive of drug sensitivity to BCL2 family inhibitors but may represent alternative, tumor-relevant mechanisms (48).

In conclusion, our analysis identified a robust association between the presence of the SIX1 mutation and elevated expression levels of *MGAM*, *PTPN14*, *STAT4*, and *KDM2B*, which were tightly associated with MEKi sensitivity in a subset of Wilms tumor samples. In contrast, although navitoclax sensitivity was observed in neuroblastoma samples, no direct correlation was found between the drug sensitivity and specific gene expression features. Validation using the GDSC2 dataset confirmed that neuroblastoma drug sensitivity to BCL2 family inhibitors and gene expression patterns are independent phenomena. Our observations strongly suggest that the specific omics signatures can be utilized to predict *in vitro* sensitivity to MEKi in Wilms tumors.

Network inference provides mechanistic context for specific drug responses and multiomics signatures in Wilms tumors

Next, we aimed to elucidate the mechanisms behind the specific drug sensitivities and the associated signatures in the Wilms tumor cases. We used the CARNIVAL pipeline (46) to construct patient-specific signaling networks using functional somatic SNVs and InDels, gene expression, gene fusions, TFs, and pathway activities. A prior knowledge network for each patient was built from the OmniPath database (47) using a constraint setting. This constraint setting refined the network individually for each sample by excluding non-expressed genes and integrating information about SNVs, InDels, and gene fusions to adjust the network structure.

To explore the relation between the MEKi trametinib and the *SIX1* mutation, we analyzed common interactions reported in the patient-specific networks of the three Wilms tumor samples harboring the MEKi-*SIX1* signature. In our study, we identified common patterns of interaction within the network by observing changes in the connectivity among its nodes (genes). This involved identifying instances in which alterations in one component, such as a gene's expression level, led to discernible changes in other connected nodes. To narrow down the amount of potentially relevant interactions, we sought interactions that were noticeably absent or exhibited no activity in the three non–*SIX1*-mutated Wilms tumors that did not show sensitivity to MEKi (**Fig. 4**). With this, we identified specific interactions unique to tumors displaying the MEKi-*SIX1* signature. We utilized the comprehensive resources available through OmniPath to elucidate the biological pathways and interactions, thereby establishing a direct relationship between these two critical nodes in our network diagram. Hence, we aimed to provide a clear evidence-based illustration of how *SIX1* and *MEK1/2* interact within the broader cellular context. This visualization was designed to elucidate the relationships among SIX1, *MAP2K1/2*, and *MAPK14* within the overall molecular network. *SIX1* and *MAPK14* were linked through *AKT1*. Several TF nodes showed a link between *AKT1* and the *MAPK14*/MEK nodes, such as *ETS1*, *ATF2*, and *MYOD1*. Moreover, *KDM2B* showed an interaction between *MPK14-TCF3* and *AKT1-ETS1* activity, which may explain the association between MEKi sensitivity, the *SIX1* mutation, and *KDM2B* overexpression.

Discussion

To improve our understanding of the molecular mechanisms associated with drug response, we applied MOFA (36) to the INFORM *ex vivo* drug-screening dataset, comprising drug-screening and omics data from 76 solid and brain tumors from pediatric patients. Using MOFA, we confirmed previously known molecular drivers of clinical heterogeneity and identified two latent factors (factors 1 and 3) as drug response patterns predominantly driven by Wilms tumor and neuroblastoma, respectively. Although this subgroup dominance limits the generalizability of these findings, it underscores the feasibility of identifying clinically actionable insights even within small and heterogeneous cohorts. Future studies with larger, subtype-specific cohorts are needed to validate these observations. Although the sample size of the tumor subgroups poses inherent limitations, the insights gained in this study provide a foundation for future studies in functional precision oncology.

The first latent factor was specific to four neuroblastoma samples, in which the factor included navitoclax sensitivity as the top-weighted drug response feature. However, our analysis did not reveal any significant correlation between navitoclax sensitivity and the expression of the genes *DUSP8*, *GATA3*, and *PHOX2B*.

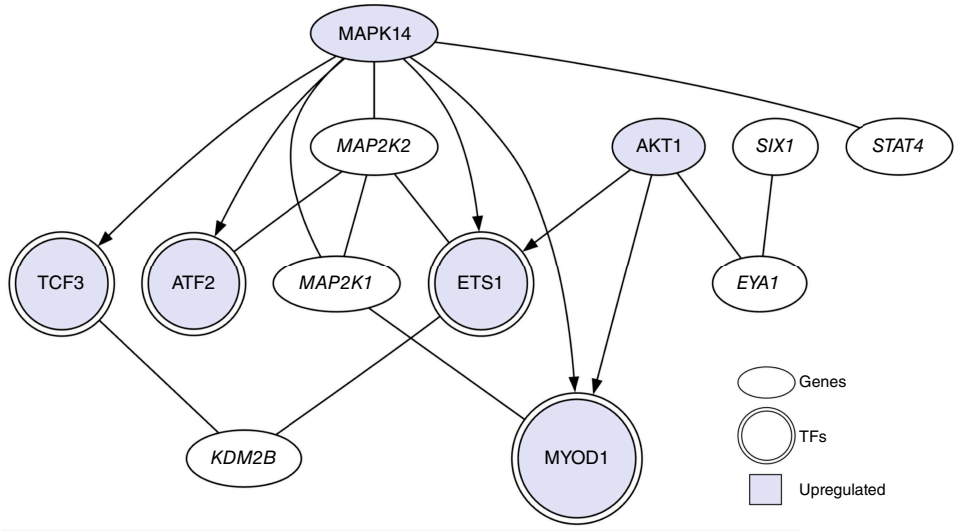

Figure 4.

Patient-specific refined signaling networks suggest potential interactions in SIX1-mutant Wilms tumors. Refined signaling networks depicted for Wilms tumor samples harboring the *SIX1* mutation. The refined networks only harbor interactions unique to the respective SIX1-mutant Wilms tumor subset, omitting interactions common to other samples or entities in the respective cohort. Blue nodes signify genes that are upregulated, meaning their activity or expression is increased. White nodes indicate OmniPath-linked genes of interest (drug targets and MOFA-associated genes). Different shapes represent distinct types of nodes within the network. Oval shapes are used to denote genes, double-lined circles highlight TFs, and inverted pentagon shapes signify predicted input perturbation nodes.

Although *GATA3* has been previously identified as a marker for neuroblastoma (49), and high expression of *DUSP8* and *PHOX2B* in neuroblastoma samples has been reported (50, 51), our findings suggest that these genes are not directly predictive of navitoclax sensitivity. These results highlight the needs to investigate alternative mechanisms driving BCL2 family inhibitor sensitivity in neuroblastoma. The observed sensitivity to navitoclax may still hold therapeutic relevance as it was also reported in our independent validation using the GDSC dataset. However, further studies are required to identify predictive markers or pathways mediating this effect.

The second latent factor was driven by three Wilms tumor samples with high sensitivity to MEKi screened within the range of clinically achievable concentrations. This factor was defined by a mutation in the *SIX1* gene and a signature of highly expressed genes (*MGAM*, *STAT4*, *PTPN14*, and *KDM2B*) in those three samples. Somatic *SIX1* mutations, and particularly a hotspot mutation (Q177R) in the homeo-domain of *SIX1*, are known to affect a subset of Wilms tumors with high proliferative potential (52, 53), but *SIX1*-mutated Wilms tumors have not yet been associated with MEKi sensitivity in the literature. This association suggests a potential therapeutic avenue and candidate biomarker although further functional studies are necessary to confirm their clinical relevance. Additionally, none of the highly expressed genes identified in this study have been previously linked to MEKi response. This suggests that not only this gene expression signature can be used as novel predictive biomarker in the future but it might also improve our understanding of the mechanisms making tumors sensitive to MEKi.

We constructed patient-specific signaling networks for the Wilms tumor samples in our cohort to put the specific multiomics signature of the SIX1-mutated, MEKi-sensitive Wilms tumors into biological context. This enabled the comparative analysis between SIX1-mutated versus SIX1 wild-type Wilms tumors, unlike the cohort-based inferred networks that provide a broad landscape. We identified common upregulated node activities in the *SIX1*-mutated samples that could potentially explain the mechanistic interplay between MEKi and the *SIX1* mutation status. Trametinib inhibits phosphorylation of regulatory sites of MAPK14 (p38α *MAPK*; ref. 54). Yu and colleagues have shown that *SIX1* induces the expression of specific cyclin genes and stimulates *MAPK* and *AKT* activity (55). *AKT1* was captured within the common nodes of the CARNIVAL network as a main regulator of the myoblast determination protein 1 (*MYOD1*), which has been reported before to be regulated by the *SIX1* gene (56). This shows that *AKT1* is linking the trametinib–MAPK14 interaction to the *AKT* pathway, hence, putatively explaining the association between trametinib sensitivity and the *SIX1* mutation. In addition, *AKT* signaling enhances the activity of the *SIX1* transcription coactivator eyes absent 1 (*Eya1*; ref. 57). The *ETS*1 (ETS proto-oncogene 1) gene was also captured as a node linking *SIX1* and *MAPK14* within the network. The effect of AKT signaling on *Eya1*, when associated with *SIX1*, points to a potentially critical pathway influencing cell proliferation and survival in Wilms tumor. The involvement of *ETS1* as a connector within this network suggests that it could play a pivotal role in mediating the effects of these interactions on cellular functions. Such insights might not only deepen our understanding of cancer biology but also highlight potential targets and unravel hypothesis around pathways associated with drug responses and therapeutic strategies. These findings emphasize the pivotal role of integrative omics analysis in precision oncology, facilitating the understanding of complex molecular interplay of therapeutic drug targets derived from individual patient's tumor profiles. Although our computational analysis has provided significant insights, it is crucial to validate these findings experimentally. Future studies should focus on functional assays to test the roles of the identified genes and pathways.

For instance, knockdown or overexpression experiments could confirm the involvement of *KDM2B*, AKT pathway, *ETS1*, and *SIX1* in MEKi sensitivity in Wilms tumors. These experimental validations are essential to confirm the computational predictions and to translate these findings into potential clinical applications.

In summary, our findings suggest a possible mechanistic interplay between MEKi, specifically trametinib, and the *SIX1* hotspot mutation. The network analysis demonstrated that *AKT1* serves as a common node linking the trametinib–*MAPK14* interaction to the *AKT* pathway, putatively explaining trametinib sensitivity of SIX1-mutated tumors. Future studies are needed to explore whether the relationship between the highly expressed genes and *SIX1* mutations is entity related, drug response related, or mechanistically regulated by *SIX1*. By exploring the potential molecular mechanisms associated with MEKi sensitivity in *SIX1*-mutated Wilms tumor samples, this study generates hypotheses that may inform future research into the therapeutic strategies and predictive markers, ultimately improving patient stratification and personalized cancer treatment in pediatric Wilms tumors.

In this study, we demonstrated the potential of integrating DSP with comprehensive multiomics analyses. The combination of these methodologies enabled us to identify potential drug sensitivity biomarkers in Wilms tumors. Although DSP elucidates pharmacologic vulnerabilities within tumors, omics analyses can provide understanding of the molecular context, furnishing insights into the biological mechanisms of these vulnerabilities. The integration of both methodologies enhances our molecular understanding of pediatric solid tumors and may contribute to identifying potential therapeutic targets in pediatric oncology.

Data Availability

WES and RNA-seq data generated by this study are available at the European Genome Archive (EGA) under accession number EGAS00001008249 and EGAS00001005112. EGA requires controlled access, and there is a corresponding Data Access Committee to determine access permissions. Access to actual data files is not managed by the EGA. Drug response data are available at https://github.com/D-Harouni/INFORM_DSP_MultiOmics_Manuscripts/. The code used to compute the asymmetric drug sensitivity score is available at https://github.com/iTReX-Shiny/iTReX.

Authors' Disclosures

R. Hernansaiz-Ballesteros reports personal fees from Tempus and other support from QuantBio (consulting) outside the submitted work. B.C. Jones reports grants from German Cancer Aid (111234) during the conduct of the study. D.T.W. Jones reports grants from various sources during the conduct of the study, as well as other support from Heidelberg Epignostix GmbH outside the submitted work. S.M. Pfister reports nonfinancial support from Epignostix GmbH and personal fees from BioSkryb outside the submitted work, as well as a patent for Mutations of Histone Proteins Associated with Proliferative Disorders (WO2013075237 A1) issued to McGill University and DKFZ, University Hospital Heidelberg, a patent for DNA Methylation Based Method for Classifying Tumor Species (EP 16 710 700.2) issued to DKFZ, University Hospital Heidelberg, a patent for Rapid Comprehensive Adaptive Nanopore Sequencing of CNS Tumors, a Proof of Concept Study (RAPID-CNS2; EP21190233) issued to DKFZ, University Hospital Heidelberg, and University of Nottingham, and a patent for Method for the Detection of a Premalignant Lesion in a Subject (submitted, EP25166938.8) and other support from University Hospital Essen Westdeutsches Tumorzentrum 2022 to until now and other support from Gesellschaft für Pädiatrische Onkologie und Hämatologie (GPOH), International Society of Paediatric Oncology (SIOP), Deutsche Gesellschaft für Neuropathologie und Neuroanatomie (DGNN), Deutsche Krebsgesellschaft (DKG), American Association for Cancer Research (AACR), and (Society for Neuro-Oncology (SNO). O. Witt reports grants from German Federal Ministry of Education and Research (BMBF), German Cancer Research Aid, and German Childhood Cancer Foundation during the conduct of the study, as well as grants from Day One Biopharma and personal fees from Ipsen and Novartis outside the submitted work. J. Saez-Rodriguez reports grants and personal fees from Pfizer, grants from GSK, and personal fees from Tempus, Moderna, Stadapharm, Astex, Owkin, Travere Therapeutics, and Grunenthal outside the submitted work. I. Oehme reports grants from German Cancer Aid, PreComb, BVD, and Day One Therapeutics during the conduct of the study. N. Jäger reports employment with Heidelberg Epignostix GmbH. M. Schlesner reports grants from Deutsche Forschungsgemeinschft (DFG) during the conduct of the study, as well as grants from German Federal Ministry of Education and Research (BMBF) outside the submitted work. No disclosures were reported by the other authors.

Authors' Contributions

D. ElHarouni: Conceptualization, formal analysis, validation, visualization, methodology, writing–original draft, writing–review and editing. **R. Hernansaiz-Ballesteros:** Resources, formal analysis, visualization, methodology, writing–review and editing. **H. Peterziel:** Resources, methodology, writing–review and editing. **G.P. Balasubramanian:** Resources, data curation, methodology. **C. Previti:** Resources, data curation, methodology. **K. Schramm:** Resources, data curation, methodology. **M. Blattner-Johnson:** Resources, data curation, methodology. **R. Kabbe:** Resources, data curation, software, methodology. **B.C. Jones:** Resources, methodology. **S. Oppermann:** Conceptualization, resources, methodology, writing–review and editing. **D.T.W. Jones:** Resources, methodology, writing–review and editing. **S.M. Pfister:** Conceptualization, funding acquisition, writing–review and editing. **O. Witt:** Conceptualization, funding acquisition, project administration, writing–review and editing. **J. Saez-Rodriguez:** Conceptualization, methodology, writing–review and editing. **I. Oehme:** Conceptualization, resources, funding acquisition, methodology, project administration, writing–review and editing. **N. Jäger:** Conceptualization, supervision, funding acquisition, writing–review and editing. **M. Schlesner:** Conceptualization, supervision, funding acquisition, writing–review and editing.

Acknowledgments

This work was supported by SFB 1389-UNITE Glioblastoma, Work Package A02 (O. Witt and D.T.W. Jones) and D02 (D. ElHarouni and M. Schlesner). The INFORM registry was supported by the German Cancer Aid (111234), the German Childhood Oncology Foundation (DKS 2014.12 and DKS 2018.18), the German Federal Ministry of Health (ZMVI1–2520IGW004), the German Federal Ministry of Education and Research (01KX2025) and Structure and Innovation Fund, Baden-Württemberg, and the generous private donation of the Scheu family. Funding support was provided by the German Cancer Consortium (DKTK, Heidelberg, Germany) via the German Cancer Research Center (DKFZ) for a molecular diagnostics group and for support to the DKFZ Genomics and Proteomics Core Facility (GPCF). Bild e.V. "Ein Herz für Kinder" has generously supported molecular analyses for non-German patients (PÄ-24151). The INFORM drug screening platform is supported by the Federal Ministry of Education and Research (16KX2025) and the Dietmar Hopp Foundation, as well as in the framework of ERA PerMed (ERAPERMED2018-121, COMPASS). We would like to thank the DDCB core facility (FIMM High Throughput Biomedicine unit, FIMM Technology Center) supported by the University of Helsinki and Biocenter Finland for their expertise in manufacturing ready-to-use drug plates for the study. We thank the DKFZ's Omics IT and Data Management Core Facility and GPCF for supporting genomic sequencing. We would like to express our sincere thanks to Carsten Maus, Erjia Wang (GPCF, DKFZ), Lena Weiser, and Gregor Warsow (Omics IT and Data Management Core Facility, DKFZ) for their highly dedicated support in data management and processing and Robert Autry (Division of Pediatric Neurooncology, DKFZ) for his sincere contribution to the INFORM bioinformatics analyses. We thank Aileen Friedenauer, Alexandra Stroh-Dege, and Marko Weidmann for their technical assistance in the DSP. Furthermore, we thank the patients and their families for their consent to collect and use tumor material and all participating INFORM sites for providing tumor tissue and clinical data. Generative artificial intelligence (ChatGPT-4, OpenAI) was used solely for language proofreading.

Note

Supplementary data for this article are available at Cancer Research Online (http://cancerres.aacrjournals.org/).

Received June 16, 2024; revised January 18, 2025; accepted August 13, 2025; posted first December 19, 2025.

References

1. World Health Organization. CureAll framework: WHO global initiative for childhood cancer: increasing access, advancing quality, saving lives. World Health Organization; 2021. p. 109. [Cited June 2025.] Available from: https://apps.who.int/iris/handle/10665/347370.
2. Howlader N, Noone AM, Krapcho M, Miller D, Bishop K, Kosary CL, et al SEER Cancer Statistics Review, 1975–2014. Bethedsa (MD): National Cancer Institute; 2017. [Cited June 2025.] Available from: https://seer.cancer.gov/csr/1975_2014/.
3. Ma X, Liu Y, Liu Y, Alexandrov LB, Edmonson MN, Gawad C, et al. Pan-cancer genome and transcriptome analyses of 1,699 paediatric leukaemias and solid tumours. Nature 2018;555:371–6.
4. Gröbner SN, Worst BC, Weischenfeldt J, Buchhalter I, Kleinheinz K, Rudneva VA, et al. The landscape of genomic alterations across childhood cancers. Nature 2018;555:321–7.
5. Pfister SM, Reyes-Múgica M, Chan JKC, Hasle H, Lazar AJ, Rossi S, et al. A summary of the inaugural WHO classification of pediatric tumors: transitioning from the optical into the molecular era. Cancer Discov 2022;12:331–55.
6. Burdach SEG, Westhoff MA, Steinhauser MF, Debatin KM. Precision medicine in pediatric oncology. Mol Cell Pediatr 2018;5:6.
7. Laetsch TW, DuBois SG, Bender JG, Macy ME, Moreno L. Opportunities and challenges in drug development for pediatric cancers. Cancer Discov 2021;11:545–59.
8. Bertacca I, Pegoraro F, Tondo A, Favre C. Targeted treatment of solid tumors in pediatric precision oncology. Front Oncol 2023;13:1176790.
9. Langenberg KPS, Looze EJ, Molenaar JJ. The landscape of pediatric precision oncology: program design, actionable alterations, and clinical trial development. Cancers (Basel) 2021;13:4324.
10. Sharma A, Debik J, Naume B, Ohnstad HO, Bathen TF, Giskeødegård GF, et al; Oslo Breast Cancer Consortium OSBREAC. Comprehensive multi-omics analysis of breast cancer reveals distinct long-term prognostic subtypes. Oncogenesis 2024;13:22.
11. Sturm D, Capper D, Andreiuolo F, Gessi M, Kölsche C, Reinhardt A, et al. Multiomic neuropathology improves diagnostic accuracy in pediatric neuro-oncology. Nat Med 2023;29:917–26.
12. Heo YJ, Hwa C, Lee G-H, Park J-M, An J-Y. Integrative multi-omics approaches in cancer research: from biological networks to clinical subtypes. Mol Cells 2021;44:433–43.
13. Liang W-W, Lu RJ-H, Jayasinghe RG, Foltz SM, Porta-Pardo E, Geffen Y, et al. Integrative multi-omic cancer profiling reveals DNA methylation patterns associated with therapeutic vulnerability and cell-of-origin. Cancer Cell 2023;41:1567–85.e7.
14. Toshimitsu K, Takano A, Fujii M, Togasaki K, Matano M, Takahashi S, et al. Organoid screening reveals epigenetic vulnerabilities in human colorectal cancer. Nat Chem Biol 2022;18:605–14.
15. Acanda De La Rocha AM, Berlow NE, Fader M, Coats ER, Saghira C, Espinal PS, et al. Feasibility of functional precision medicine for guiding treatment of relapsed or refractory pediatric cancers. Nat Med 2024;30:990–1000.
16. Liebers N, Bruch P-M, Terzer T, Hernandez-Hernandez M, Paramasivam N, Fitzgerald D, et al. Ex vivo drug response profiling for response and outcome prediction in hematologic malignancies: the prospective non-interventional SMARTrial. Nat Cancer 2023;4:1648–59.
17. Lu J, Cannizzaro E, Meier-Abt F, Scheinost S, Bruch P-M, Giles HAR, et al. Multi-omics reveals clinically relevant proliferative drive associated with mTOR-MYC-OXPHOS activity in chronic lymphocytic leukemia. Nat Cancer 2021;2:853–64.
18. Leo IR, Aswad L, Stahl M, Kunold E, Post F, Erkers T, et al. Integrative multi-omics and drug response profiling of childhood acute lymphoblastic leukemia cell lines. Nat Commun 2022;13:1691.
19. Wang Z, Li Y, Zhao W, Jiang S, Huang Y, Hou J, et al. Integrative multi-omics and drug–response characterization of patient-derived prostate cancer primary cells. Signal Transduct Target Ther 2023;8:175.
20. Worst BC, van Tilburg CM, Balasubramanian GP, Fiesel P, Witt R, Freitag A, et al. Next-generation personalised medicine for high-risk paediatric cancer patients – the INFORM pilot study. Eur J Cancer 2016;65:91–101.
21. van Tilburg CM, Pfaff E, Pajtler KW, Langenberg KPS, Fiesel P, Jones BC, et al. The pediatric precision oncology INFORM registry: clinical outcome and benefit for patients with very high-evidence targets. Cancer Discov 2021;11:2764–79.
22. Peterziel H, Jamaladdin N, ElHarouni D, Gerloff XF, Herter S, Fiesel P, et al. Drug sensitivity profiling of 3D tumor tissue cultures in the pediatric precision oncology program INFORM. NPJ Precis Oncol 2022;6:94.
23. Heipertz A-E, Pajtler KW, Pfaff E, Schramm K, Blattner-Johnson M, Milde T, et al. Outcome of children and adolescents with relapsed/refractory/progressive malignancies treated with molecularly informed targeted drugs in the pediatric precision oncology registry INFORM. JCO Precis Oncol 2023;7:e2300015.
24. ElHarouni D, Berker Y, Peterziel H, Gopisetty A, Turunen L, Kreth S, et al. iTReX: interactive exploration of mono- and combination therapy dose response profiling data. Pharmacol Res 2022;175:105996.
25. Reisinger E, Genthner L, Kerssemakers J, Kensche P, Borufka S, Jugold A, et al. OTP: an automatized system for managing and processing NGS data. J Biotechnol 2017;261:53–62.
26. ICGC/TCGA Pan-Cancer Analysis of Whole Genomes Consortium. Pan-cancer analysis of whole genomes. Nature 2020;578:82–93.
27. Li H, Handsaker B, Wysoker A, Fennell T, Ruan J, Homer N, et al. The Sequence Alignment/Map format and SAMtools. Bioinformatics 2009;25:2078–9.
28. Li H. A statistical framework for SNP calling, mutation discovery, association mapping and population genetical parameter estimation from sequencing data. Bioinformatics 2011;27:2987–93.
29. Jones DTW, Hutter B, Jäger N, Korshunov A, Kool M, Warnatz H-J, et al. Recurrent somatic alterations of FGFR1 and NTRK2 in pilocytic astrocytoma. Nat Genet 2013;45:927–32.
30. Rimmer A, Phan H, Mathieson I, Iqbal Z, Twigg SRF, Wilkie AOM, McVeanG, et al; WGS500 Consortium. Integrating mapping-assembly- and haplotype-based approaches for calling variants in clinical sequencing applications. Nat Genet 2014;46:912–8.
31. Wang K, Li M, Hakonarson H. ANNOVAR: functional annotation of genetic variants from high-throughput sequencing data. Nucleic Acids Res 2010;38:e164.
32. Talevich E, Shain AH, Botton T, Bastian BC. CNVkit: genome-wide copy number detection and visualization from targeted DNA sequencing. PLoS Comput Biol 2016;12:e1004873.
33. Dobin A, Davis CA, Schlesinger F, Drenkow J, Zaleski C, Jha S, et al. STAR: ultrafast universal RNA-seq aligner. Bioinformatics 2013;29:15–21.
34. Liao Y, Smyth GK, Shi W. featureCounts: an efficient general purpose program for assigning sequence reads to genomic features. Bioinformatics 2014;30:923–30.
35. Uhrig S, Ellermann J, Walther T, Burkhardt P, Fröhlich M, Hutter B, et al. Accurate and efficient detection of gene fusions from RNA sequencing data. Genome Res 2021;31:448–60.
36. Argelaguet R, Arnol D, Bredikhin D, Deloro Y, Velten B, Marioni JC, et al. MOFA+: a statistical framework for comprehensive integration of multi-modal single-cell data. Genome Biol 2020;21:111.
37. Sondka Z, Bamford S, Cole CG, Ward SA, Dunham I, Forbes SA. The COSMIC Cancer Gene Census: describing genetic dysfunction across all human cancers. Nat Rev Cancer 2018;18:696–705.
38. Chakravarty D, Gao J, Phillips S, Kundra R, Zhang H, Wang J, et al. OncoKB: a precision oncology knowledge base. JCO Precis Oncol 2017;1:PO.17.00011.
39. Cotto KC, Wagner AH, Feng Y-Y, Kiwala S, Coffman AC, Spies G, et al. DGIdb 3.0: a redesign and expansion of the drug-gene interaction database. Nucleic Acids Res 2018;46:D1068–73.
40. Mootha VK, Lindgren CM, Eriksson K-F, Subramanian A, Sihag S, Lehar J, et al. PGC-1alpha-responsive genes involved in oxidative phosphorylation are coordinately downregulated in human diabetes. Nat Genet 2003;34:267–73.
41. Subramanian A, Tamayo P, Mootha VK, Mukherjee S, Ebert BL, Gillette MA, et al. Gene set enrichment analysis: a knowledge-based approach for interpreting genome-wide expression profiles. Proc Natl Acad Sci U S A 2005;102:15545–50.
42. Carlson M. org.Hs.eg.db: Genome wide annotation for Human. R package version 3.8.2. 2019. [Cited May 2024.] Available from: https://bioconductor.org/packages/org.Hs.eg.db
43. Argelaguet R, Velten B, Arnol D, Dietrich S, Zenz T, Marioni JC, et al. Multi-omics factor analysis-a framework for unsupervised integration of multi-omics data sets. Mol Syst Biol 2018;14:e8124.
44. Schubert M, Klinger B, Klünemann M, Sieber A, Uhlitz F, Sauer S, et al. Perturbation-response genes reveal signaling footprints in cancer gene expression. Nat Commun 2018;9:20.

45. Garcia-Alonso L, Holland CH, Ibrahim MM, Turei D, Saez-Rodriguez J. Benchmark and integration of resources for the estimation of human transcription factor activities. Genome Res 2019;29:1363–75.
46. Liu A, Trairatphisan P, Gjerga E, Didangelos A, Barratt J, Saez-Rodriguez J. From expression footprints to causal pathways: contextualizing large signaling networks with CARNIVAL. NPJ Syst Biol Appl 2019;5:40.
47. Türei D, Korcsmáros T, Saez-Rodriguez J. OmniPath: guidelines and gateway for literature-curated signaling pathway resources. Nat Methods 2016;13:966–7.
48. Durbin AD, Zimmerman MW, Dharia NV, Abraham BJ, Iniguez AB, Weichert-Leahey N, et al. Selective gene dependencies in MYCN-amplified neuroblastoma include the core transcriptional regulatory circuitry. Nat Genet 2018;50:1240–6.
49. Wiles AB, Karrs JX, Pitt S, Almenara J, Powers CN, Smith SC. GATA3 is a reliable marker for neuroblastoma in limited samples, including FNA Cell Blocks, core biopsies, and touch imprints. Cancer Cytopathol 2017;125:940–6.
50. Zafar A, Wang W, Liu G, Wang X, Xian W, McKeon F, et al. Molecular targeting therapies for neuroblastoma: progress and challenges. Med Res Rev 2021;41:961–1021.
51. Nunes-Xavier C, Zaldumbide L, Aurtenetxe O, López-Almaraz R, López J, Pulido R. Dual-specificity phosphatases in neuroblastoma cell growth and differentiation. Int J Mol Sci 2019;20:1170.
52. Wegert J, Ishaque N, Vardapour R, Geörg C, Gu Z, Bieg M, et al. Mutations in the SIX1/2 pathway and the DROSHA/DGCR8 miRNA microprocessor complex underlie high-risk blastemal type Wilms tumors. Cancer Cell 2015;27:298–311.
53. Walz AL, Ooms A, Gadd S, Gerhard DS, Smith MA, Guidry Auvil JM, et al. Recurrent DGCR8, DROSHA, and SIX homeodomain mutations in favorable histology Wilms tumors. Cancer Cell 2015;27:286–97.
54. Basken J, Stuart SA, Kavran AJ, Lee T, Ebmeier CC, Old WM, et al. Specificity of phosphorylation responses to mitogen activated protein (MAP) kinase pathway inhibitors in melanoma cells. Mol Cell Proteomics 2018;17:550–64.
55. Yu Y, Davicioni E, Triche TJ, Merlino G. The homeoprotein Six1 transcriptionally activates multiple protumorigenic genes but requires ezrin to promote metastasis. Cancer Res 2006;66:1982–9.
56. Liu Y, Chakroun I, Yang D, Horner E, Liang J, Aziz A, et al. Six1 regulates MyoD expression in adult muscle progenitor cells. PLoS One 2013;8:e67762.
57. Sun Y, Kaneko S, Li XK, Li X. The PI3K/Akt signal hyperactivates Eya1 via the SUMOylation pathway. Oncogene 2015;34:2527–37.